International Journal of Nanomedicine

Dovepress
open access to scientific and medical research

Open Access Full Text Article

ORIGINAL RESEARCH

Targeted Delivery of Geraniol via Hyaluronic Acid-Conjugation Enhances Its Anti-Tumor Activity Against Prostate Cancer

Han Yu[1–4], Na Ning[1–3], Fujin He[5], Jiao Xu[6], Han Zhao[5], Shaofeng Duan[5,7], Yunqi Zhao[1–4]

[1]College of Science, Mathematics and Technology, Wenzhou-Kean University, Wenzhou, Zhejiang Province, 325060, People's Republic of China; [2]Wenzhou Municipal Key Laboratory for Applied Biomedical and Biopharmaceutical Informatics, Wenzhou-Kean University, Wenzhou, Zhejiang, 325060, People's Republic of China; [3]Zhejiang Bioinformatics International Science and Technology Cooperation Center, Wenzhou-Kean University, Wenzhou, Zhejiang, 325060, People's Republic of China; [4]Dorothy and George Hennings College of Science, Mathematics and Technology, Kean University, Union, NJ, 07083, USA; [5]School of Pharmacy, Henan University, Kaifeng, Henan, 475004, People's Republic of China; [6]Wenzhou Institute, University of Chinese Academy of Sciences, Wenzhou, Zhejiang, 325001, People's Republic of China; [7]The First Affiliated Hospital of Henan University, Kaifeng, Henan, 475004, People's Republic of China

Correspondence: Yunqi Zhao, College of Science, Mathematics and Technology, Wenzhou-Kean University, Wenzhou, Zhejiang, 325060, People's Republic of China, Tel +86 577 5587 0000, Fax +86 577 5587 0101, Email yuzhao@kean.edu; Shaofeng Duan, School of Pharmacy, Henan University, Kaifeng, Henan, 475004, People's Republic of China, Fax +86 371 2286 5974, Email sduan@henu.edu.cn

Background: Targeted delivery systems have been developed to improve cancer treatment by reducing side effects and enhancing drug efficacy. Geraniol, a natural product, has demonstrated promising anti-cancer effects in various cancer types, including prostate cancer, which is the most commonly diagnosed cancer in men. Hyaluronic acid (HA), a natural carrier targeting CD44-positive prostate cancer cells, can be utilized in a targeted delivery system.

Purpose: This study investigated the efficacy of a conjugate of HA and geraniol linked via a disulfide bond linker (HA-SS-Geraniol) in prostate cancer.

Materials and Methods: The cytotoxicity of HA-SS-Geraniol was evaluated on human PC-3 prostate cancer cells. Flow cytometry was used to assess its effects on mitochondrial membrane potential, apoptosis, and cell cycle arrest. Additionally, proteomic analysis was conducted to explore the underlying mechanism of action induced by HA-SS-Geraniol treatment. A subcutaneous xenograft tumor model was established in nude mice to evaluate the toxicity and efficacy of HA-SS-Geraniol in vivo.

Results: The results demonstrated that HA-SS-Geraniol exhibited potent cytotoxicity against PC-3 prostate cancer cells by inducing mitochondrial membrane potential loss and apoptosis in vitro. The proteomic analysis further supported the hypothesis that HA-SS-Geraniol induces cell death through mitochondria-mediated apoptosis, as evidenced by differential protein expression. The in vivo mouse model confirmed the safety of HA-SS-Geraniol and its ability to inhibit tumor growth.

Conclusion: HA-SS-Geraniol holds promise as a biologically safe and potentially effective therapeutic agent for prostate cancer treatment. Its targeted delivery system utilizing HA as a carrier shows potential for improving the efficacy of geraniol in cancer therapy.

Keywords: geraniol, hyaluronic acid, prostate cancer, nanoparticle, proteomics

Introduction

Prostate cancer has become the second most prevalent cancer among men globally.[1] Due to the aging population, dietary changes, and environmental factors, the incidence of prostate cancer is rapidly rising, making it one of the fastest-growing malignant tumors.[2] Traditional chemotherapeutic drugs potently kill both cancerous and healthy tissues, leading to severe side effects in patients and negatively impacting their immune system, ultimately affecting their chemotherapy prognosis.[3,4] Therefore, there is an urgent need to develop new therapeutics and advanced techniques to treat prostate cancer.

Received: 15 October 2023
Accepted: 22 December 2023
Published: 6 January 2024

The tumor microenvironment (TME) is crucial to tumor development and drug resistance. Tumors possess unique structures and microenvironments that differ from normal tissues. For instance, a high glutathione (GSH) level is a distinctive feature of the TME.[5] GSH is a vital antioxidant in the antioxidant system that eliminates reactive oxygen species highly expressed in the tumor environment, preventing cell death caused by oxidative stress from DNA, protein, and lipid damage.[6] Disulfide bonds can be rapidly broken down in tumors through thiol-disulfide exchange reactions in the highly expressed antioxidant in the tumor tissue.[7] This characteristic has been incorporated into drug coupling design to develop novel drug delivery systems for cancer-targeted therapy. Targeted therapy is a critical area of research in cancer treatment, and its highly specific approach is considered an essential way to enhance tumor treatment efficacy and minimize adverse reactions to chemotherapy. Nanotechnology has significant advantages in improving the druggability of small molecules and is widely used in the targeted delivery of anti-cancer drugs. Moreover, numerous studies have demonstrated that nano-drug delivery systems designed for the tumor microenvironment exhibit better safety and improved drug availability.[8,9]

HA is a natural polysaccharide, a water-soluble, biodegradable polymer widely distributed in the human body. Given its excellent biological safety, biodegradability, and non-immunogenicity, it has extensive applications in drug delivery system research.[10,11] CD44 is one of the cell surface receptors for HA, a glycoprotein on the cell surface that participates in various cell functions, including cell proliferation, differentiation, and metastasis of cancer cells.[12] Additionally, it is one of the biomarkers to distinguish normal cells from cancer cells.[13] Studies have demonstrated that CD44 plays a crucial role in the proliferation, migration, and invasion of prostate cancer cells.[14] The expression level of CD44 on the surface of prostate cancer cells is linked to the transition and metastasis degree of epithelial-mesenchymal cells. It can predict cancer treatment effects and facilitate personalized clinical treatment decisions for prostate cancer.[15] Using HA as a carrier, chemotherapy drugs can be actively delivered to CD44-positive prostate cancer cells.

Natural products are extensively utilized in cancer research due to their minimal side effects and high biological activities.[16] Essential oils, commonly found in cosmetics and foods, are also being explored in the pharmaceutical field due to their natural derivative properties.[17] Geraniol, an olefinic terpene initially isolated from palmarosa, has demonstrated potent antioxidant effects.[18] Choi et al determined that geraniol exhibited high free radical scavenging ability in vitro, equivalent to 87.7% of Trolox (235.9 mg of Trolox equiv/mL).[19] Geraniol has also displayed excellent anti-cancer effects in various cancer models, including breast, lung, colon, pancreatic, skin, liver, kidney, and prostate.[20–23] Carnesecchi et al utilized a mouse model with TC-118 human tumors to compare the dominant anti-tumor efficacy of geraniol with 5-fluorouracil.[22] Several studies have demonstrated that geraniol induces apoptosis and autophagy and disrupts the cell cycle pathway in prostate cancer cells.[27,28]

In this study, the anti-cancer properties of the HA-SS-Geraniol conjugate against prostate cancer were assessed. Protein profiling was conducted to gain further insights into the functional proteins and underlying mechanisms of drug action.

Materials and Methods

Materials

Geraniol was commercially bought from Aladdin Bio-Chem Technology Co., Ltd. (Shanghai, China). F12K medium, fetal bovine serum (FBS), and penicillin-streptomycin (PS) were purchased from Solarbio Science & Technology Co., Ltd. (Beijing, China), Corning Inc. (Auckland, New Zealand), and Gibco, Thermo Fisher Scientific Inc., respectively. HA-SS-geraniol was provided by Dr. Duan's lab at Henan University and synthesized as described previously.[29] The human PC-3 prostate cancer cell line was purchased from the Peking Union Medical College Cell Culture Center (1101HUM-PUMC000115) (Beijing, China). The Cell Counting Kit-8 (CCK-8) and Annexin V-FITC Apoptosis Detection Kit were purchased from Elabscience Biotechnology Co., Ltd. (Wuhan, China). The Cellstain® Rhodamine 123 (Rh-123) Kit was procured from Sigma-Aldrich, Merck Ltd. The PI/RNase Staining Kit was purchased from Dojindo Molecular Technologies, Inc.

Cytotoxicity

Human prostate cancer cells, PC-3, were cultured in an F12K medium containing 10% FBS and 1% PS. The cells were seeded in 96-well plates and incubated at 37 °C and 5% CO_2 with 95% humidity. The cells were allowed to grow overnight before being treated with different final concentrations of geraniol and HA-SS-Geraniol conjugates. After 48 hours of treatment, 10 μL of CCK-8 solution was added. After another 4 hours of incubation at 37 °C, the optical densities (O.D.) were measured at 450 nm and 650 nm by a microplate reader (VarioskanFlash-4.00.53, Thermo Scientific Inc.).

Mitochondrial Membrane Potential Loss

The mitochondrial membrane potential loss was determined using the Rh-123 Kit. The PC-3 cells were seeded in 6-well plates overnight. Then, 2 mM of geraniol and HA-SS-Geraniol, containing 2 mM geraniol, were added. After 24 h of treatment, the cells were collected. Later, the collected cells were resuspended in a 20 μM Rh-123-F12K medium mixture and incubated at 37 °C for 30 minutes. Finally, the cells were washed and resuspended in phosphate (PBS) buffer at a density of 1×10^6 cells/mL for mitochondrial membrane potential loss determination using flow cytometry (NovoCyte 3000, Agilent; software: Flowjo_V10, Novoexpress 1.5.0, Agilent, CA, USA).

Cell Apoptosis Induction

The Annexin V-FITC Apoptosis Detection Kit was used to study the apoptotic effects. The PC-3 cells were seeded in 6-well plates and treated with 2 mM geraniol and HA-SS-Geraniol for 24 hours. The cells were collected and washed using PBS. 1× Annexin V Binding Solution was added to resuspend the cell pellet. Five microliters of Annexin V-FITC conjugate and 5 μL of propidium iodide (PI) solution were added and incubated in the dark at room temperature for 15 min. Five hundred microliters of 1× Annexin V Binding Solution were added to the cell suspension. Apoptosis induction was evaluated by flow cytometry.

Cell Cycle Arrest

The cell distributions were tested using PI/RNase Staining Kits. Six-well plates were used for PC-3 cell seeding. Then, the cells were treated with 2 mM geraniol and HA-SS-Geraniol for 24 hours and collected. Later, the cell pellets were washed using PBS and fixed with −20 °C cooled 70% ethanol at 4 °C for 2 hours. After fixation, the cells were washed and treated with RNase. Sequentially, the cells were dyed with PI and put in an environment of 37 °C and 4 °C for 30 minutes each. Finally, a nylon mesh was used to filter the cells, and then the cell suspensions were tested using flow cytometry.

Proteomics Analysis

Sample Preparation

The human PC-3 prostate cancer cells were cultured in 150T flasks and treated with 2 mM geraniol and HA-SS-Geraniol for 24 hours. Then, the cells were washed with pre-cooled PBS and harvested. Later, the cells experienced a 5-minute quick freeze in liquid nitrogen. Five parallel samples for each group were established and kept in a −80 °C refrigerator for the following uses.

Protein Extraction and Labeling

The samples were lysed, and proteins were extracted using SDT buffer containing 4% SDS, 100 mM Tris-HCl, and 1 mM DTT at pH 7.6. Protein quantification was performed using the BCA Protein Assay Kit (Bio-Rad, USA). Each sample was mixed with a 5× loading buffer and boiled for 5 minutes. Then, 20 μg of protein was loaded onto a 12.5% SDS–PAGE gel. Electrophoresis was conducted at a constant 180 V current for 45 minutes. Protein bands were visualized via Coomassie Blue R-250 staining. For protein digestion, the filter-aided sample preparation (FASP) procedure described by Mann et al was followed.[30] The digested peptides were desalted using an MCX cartridge. They were then concentrated by vacuum centrifugation and reconcentrated in 40 μL of 0.1% (v/v) formic acid.

According to manufacturer instructions, protein labeling was performed using the TMT reagent (Thermo Scientific). One hundred micrograms of peptide mixture was labeled per sample.

High-pH Reversed-Phase Fractionation and LC-MS/MS Analysis

The TMT-labeled peptide mixtures were fractionated before LC-MS/MS analysis to reduce sample complexity. Fractionation was performed using a Pierce^{TM} High pH Reversed-Phase Peptide Fractionation Kit. The peptide mixtures were reconstituted and acidified with 0.1% trifluoroacetic acid (TFA) solution, then loaded onto pre-equilibrated high pH reversed-phase fractionation spin columns. The collected peptides were attached to the hydrophobic resin under aqueous conditions, and then the column was washed with water using low-speed centrifugation to desalt. The columns were washed, and a step gradient of aqueous and acetonitrile solutions was applied to elute peptides into separate fractions sequentially. This method eluted the peptides into different fractions collected through centrifugation. The collected fractions were then vacuum-dried and lyophilized using 12 μL of a 0.1% formic acid solution. The selected peptide fractions were analyzed using LC-MS/MS. The system consisted of a Q Exactive mass spectrometer coupled to an Easy nLC nano-liquid chromatograph (Thermo Scientific, Germany). The peptides were introduced onto a reverse phase trap column (Thermo Scientific Acclaim PepMap100, 100 μm × 2 cm, nanoViper C18) that was connected to the C18-reversed phase analytical column (Thermo Scientific Easy Column, 10 cm long, 75 μm inner diameter, 3 μm resin). Sample loading was done using buffer A (0.1% formic acid). Peptide separation was achieved using a linear gradient of buffer B (84% acetonitrile and 0.1% formic acid) at a controlled flow rate of 300 nl/min. The mass spectrometer was operated in positive ion mode. MS data were obtained using a method that dynamically selected the most abundant precursor ions from the survey scan range of 300–1800 m/z for HCD fragmentation. The parameter settings are as follows: 1e6 for the automatic gain control (AGC) target, 50 ms for the maximum inject time, 30.0 s for the dynamic exclusion duration, a resolution of 60,000 at m/z 200 for survey scans, a resolution of 15,000 at m/z 200 for HCD spectra, 1.5 m/z for the isolation width for precursor ion selection, 30 eV for the normalized collision energy used for fragmentation, and 0.1% for the underfill ratio.

Protein Identification and Quantitation

The MS raw data was identified and quantified using Proteome Discoverer 2.4 software, including the MASCOT engine (Matrix Science, London, UK; version 2.2). The parameters were as follows: ±20 ppm for peptide mass tolerance, 0.1 Da for fragment mass tolerance, Decoy for database pattern, and a peptide false discovery rate (FDR) of less than or equal to 0.01.

Bioinformatics Analysis

Hierarchical clustering analysis was performed using Cluster 3.0 (http://bonsai.hgc.jp/~mdehoon/software/cluster/software.htm) and Java Treeview software (http://jtreeview.sourceforge.net). Protein subcellular localization prediction was evaluated using CELLO (http://cello.life.nctu.edu.tw/). Protein sequences, pathways, and functional annotations were identified using the NCBI BLAST+ client software (NCBI-blast-2.2.28+-win32.exe), InterProScan, and the online Kyoto Encyclopedia of Genes and Genomes (KEGG) database (http://geneontology.org/). Blast2GO (https://www.blast2go.com/) was utilized for gene ontology (GO) term mapping and sequence annotation. R scripts were used for the GO annotation division. Enrichment analysis was conducted using Fisher's exact test and Benjamini-Hochberg correction. Protein-protein interaction (PPI) networks were studied and visualized with the assistance of the IntAct molecular interaction database (http://www.ebi.ac.uk/intact/) and STRING software (http://string-db.org/).

In vivo Efficacy Study

Male nude mice were purchased from the Zhejiang Experimental Animal Center (Hangzhou, China), and experienced a few days of acclimatization once they arrived. The mice were all equally aged (6–8 weeks) and weighed around 20 g. They were raised in a sterile room with a 12-hour light/dark cycle. The mice were equally fed with autoclaved water and sterilizable food. All animal experimental procedures complied with the Guide for the Care and Use of Laboratory Animals at the Wenzhou Institute, University of the Chinese Academy of Sciences, and were approved by the

Experimental Animal Ethics Committee of the Wenzhou Institute, University of the Chinese Academy of Sciences (approval no. WIUCAS22121503).

The mice were randomly divided into 3 groups: the control, geraniol, and HA-SS-Geraniol groups. The mice were established subcutaneous xenograft tumor models on the right back with 2×10^6 human PC-3 prostate cancer cells diluting in PBS. After the xenograft model was developed, the mice experienced a 5-week treatment with solvent control, 100 mg/kg of geraniol, and HA-SS-Geraniol (100 mg/kg geraniol equivalent) for each group. The treatments were taken, and the tumor volumes were calculated under the formula 0.5236 x length x width^2 every 48 hours. The tumor growth inhibitory ratio was under the formula $1-\left(\frac{\text{tumor volume}_{\text{treatedgroup}}}{\text{tumor volume}_{\text{controlgroup}}}\right)\times 100\%$

Statistical Analysis

GraphPad Prism 10.0.0 (GraphPad Software, San Diego, USA) was utilized for statistical analysis. The data were expressed as Mean ± Standard Deviation (SD) or standard error of the mean (SEM). Group comparisons were conducted using the Student's *t*-test, and significance was determined at $p < 0.05$.

Results

Cytotoxicity

The anti-cancer effects of geraniol and HA-SS-Geraniol were evaluated on PC-3 cells. The results showed that HA did not cause cytotoxicity in PC-3 cells. The IC_{50} of geraniol was 13.95 mM (Figure 1). Furthermore, the IC_{50} of HA-SS-Geraniol was over thirty-fold lower than that of the geraniol group, with a value of 425.3 μM. HA-SS-Geraniol presented a high potential for anti-prostate cancer effects.

Mitochondrial Membrane Potential Loss

Mitochondrial potential loss rates could be determined using lipophilic cations like Rh-123. It could label living mitochondria and present them by fluorescence intensity. After geraniol and HA-SS-Geraniol treatments, the mitochondrial membrane potential loss rate increased from 0.98 ± 0.03% in the control group to 1.77 ± 0.10% in the geraniol group and 21.90 ± 1.37% in the HA-SS-Geraniol group (Figure 2A). HA-SS-Geraniol significantly enhanced mitochondrial membrane potential loss effects (Figure 2B).

Cell Apoptosis Induction

The apoptotic effects of geraniol and HA-SS-Geraniol on PC-3 cells were studied using flow cytometry. The FITC-conjugated Annexin V dye and propidium iodide (PI) dye were used to label the apoptotic cells and differentiate the early and late apoptotic cells. After treatments with 2 mM of geraniol and HA-SS-Geraniol, the geraniol group did not show a significant difference with an apoptotic rate of 5.13 ± 0.45% compared with a control group of 5.54 ± 0.23%. However,

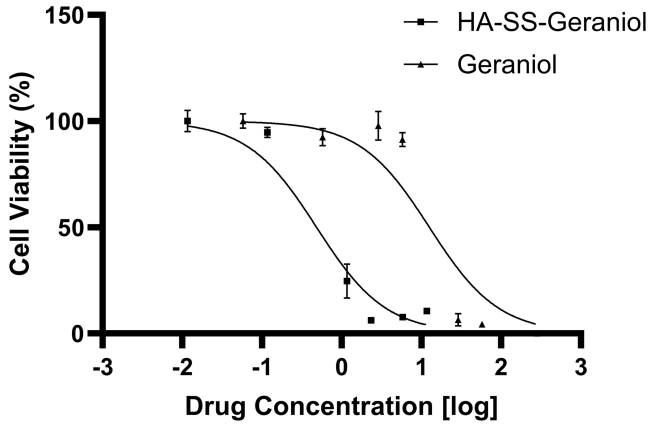

Figure 1 Cell viability analysis of PC-3 cells after treatment with geraniol or HA-SS-geraniol for 48 hours. (Mean ± SD; n = 3; * p < 0.05).

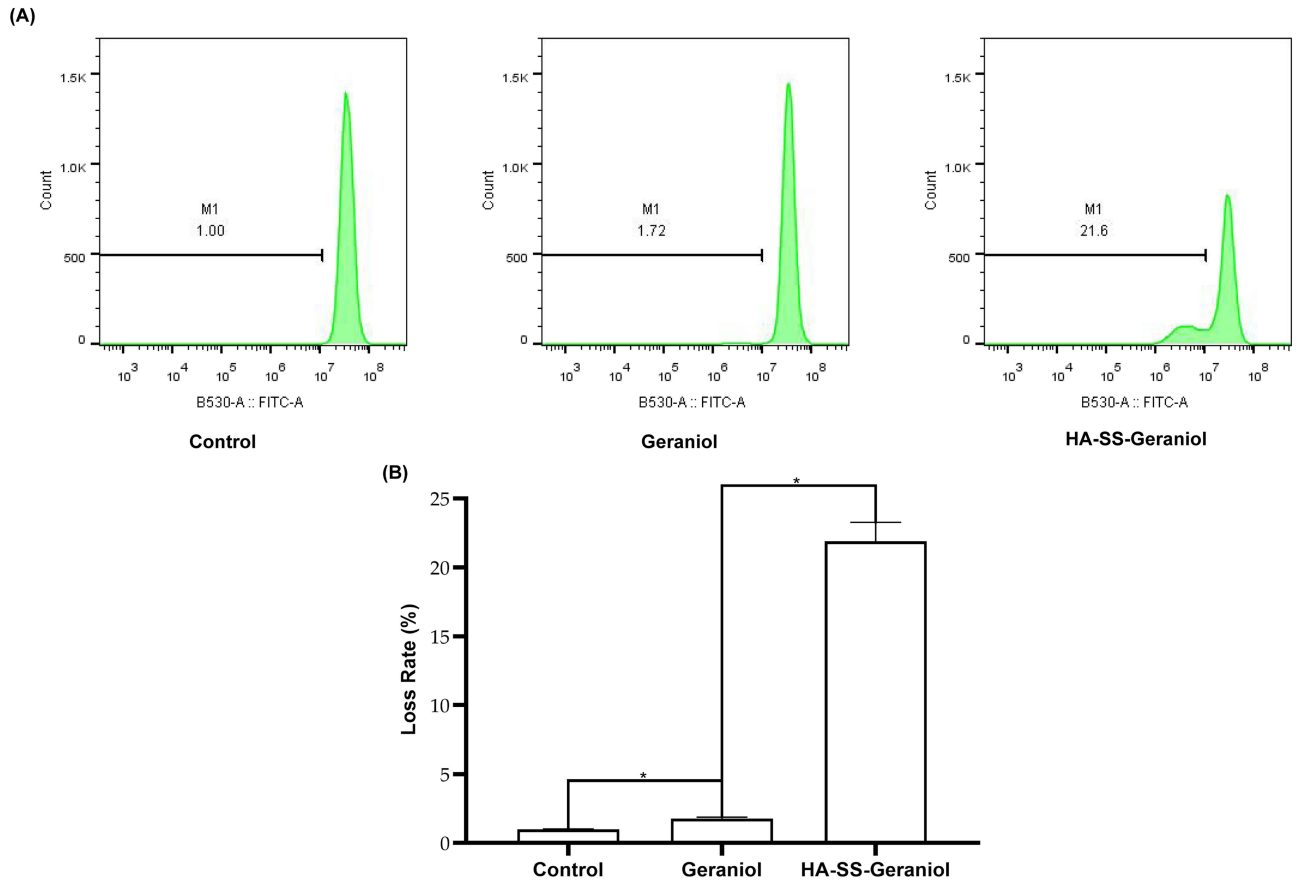

Figure 2 Representative results of mitochondrial membrane potential loss in PC-3 cells after 2 mM geraniol and HA-SS-geraniol treatments by flow cytometry (**A**) and statistical analysis of membrane potential loss (Mean ± SD; n = 3; * $p < 0.05$) (**B**).

the apoptotic rate after HA-SS-Geraniol treatment was 48.50 ± 0.10%, nearly 8-fold higher than the control group (Figure 3A and B).

Cell Cycle Arrest

Flow cytometry was used to calculate the cell distribution after treatment with geraniol and HA-SS-Geraniol. PI is a red fluorescent dye that can bind to DNA and is used to divide the cell proportion of each phase according to the fluorescent intensity. The proportions of G_0/G_1, G_2, and S phases did not show a significant difference between the control group and the geraniol group. The treatment with HA-SS-Geraniol arrested the cells in the G_2 phase (21.97%) compared with the control group (9.55%) and the geraniol group (9.00%) (Figure 4).

Proteomic Profiling of Human Prostate PC-3 Cells After Treatment with Geraniol and HA-SS-Geraniol

The proteomic analysis was conducted to investigate the changes in the proteome of PC-3 cells following treatments with geraniol and HA-SS-Geraniol. All samples were detected, collected, and analyzed, resulting in the identification of a total of 8087 proteins and 91,164 peptides. Based on the volcano plot, 352 proteins were down-regulated and 366 were up-regulated, comparing the geraniol and HA-SS-Geraniol treatment groups (Figure 5A). A heatmap was generated using the hierarchical cluster to examine the differential expression of proteins between the groups (Figure 5B). The heatmap revealed high similarity within clusters of samples from the same treatment while showing low similarity between the different treatment groups.

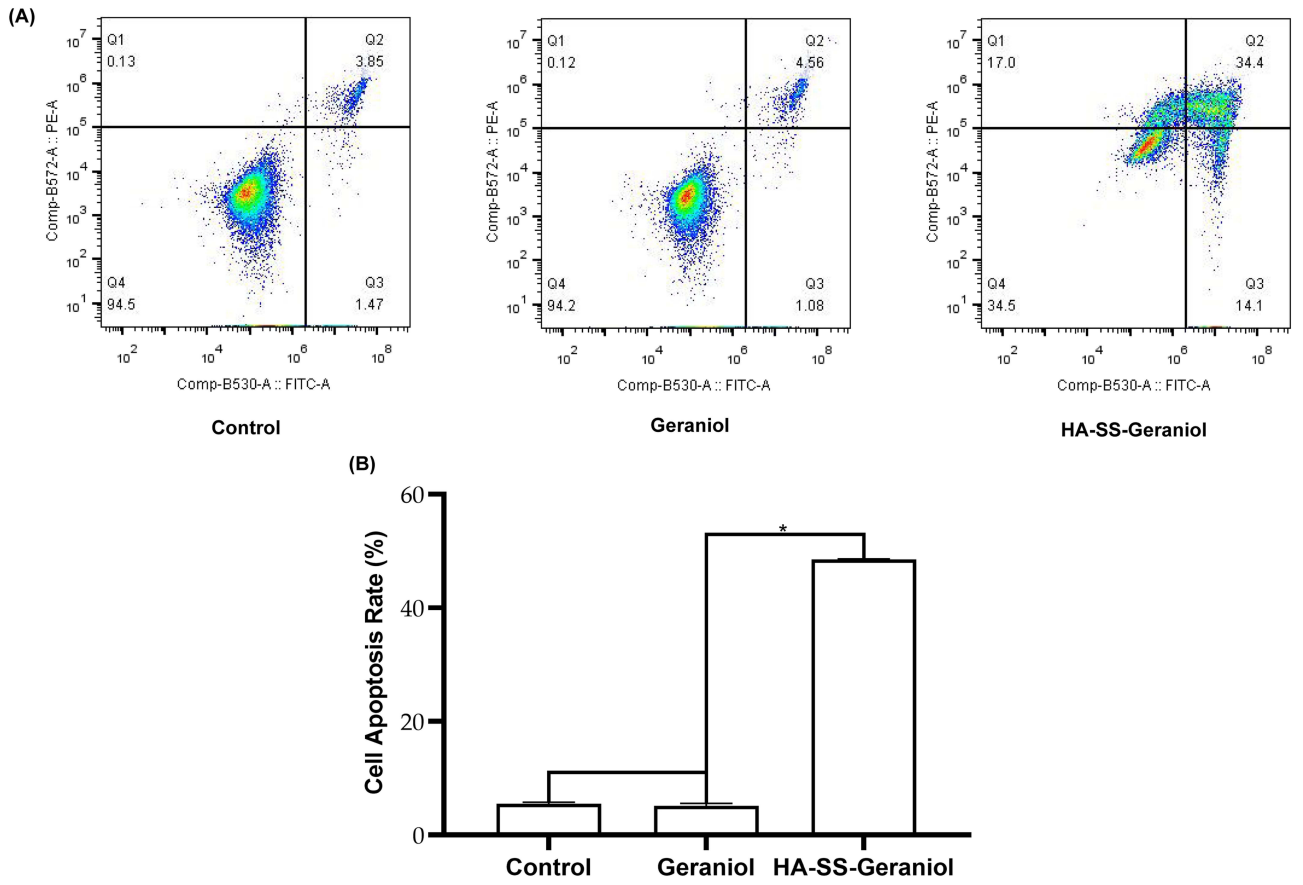

Figure 3 Representative results of apoptotic induction in PC-3 cells after 2 mM geraniol and HA-SS-geraniol treatments by flow cytometry (**A**) and statistical analysis of apoptosis rate (Mean ± SD; n = 3; * $p < 0.05$) (**B**).

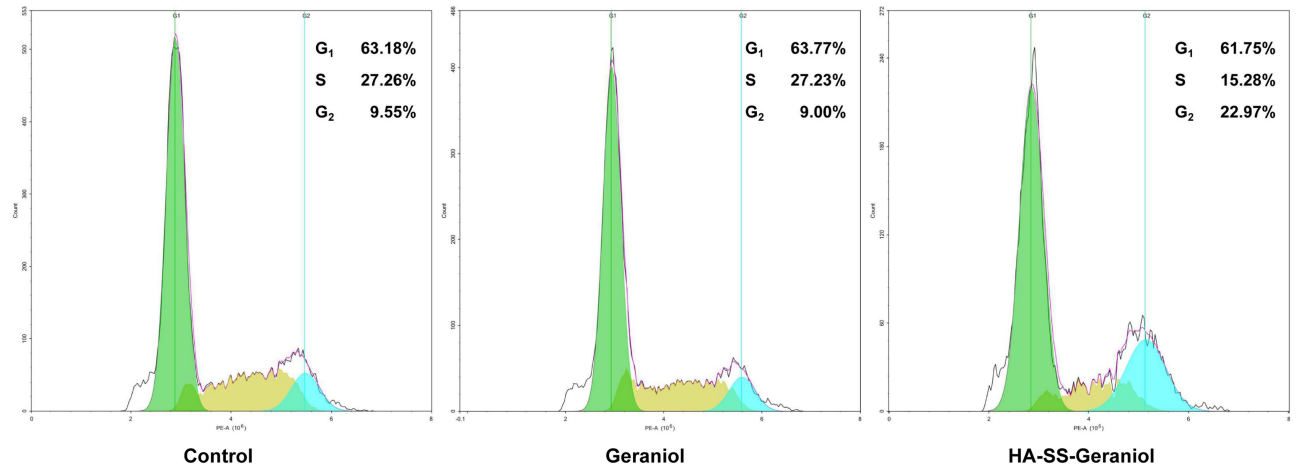

Figure 4 Representative results of cell distribution in PC-3 cells after 2 mM geraniol and HA-SS-geraniol treatments.

Subcellular Localization and Functional and Pathway Enrichment Analysis of the Differential Proteins

Proteins play various functions in different organelles. Differential proteins were analyzed for subcellular localization using the CELLO software to investigate their functions in specific organelles. The pie chart demonstrates that most differential proteins were located in the nucleus, mitochondria, and cytoplasm (Figure 6A). To gain a comprehensive understanding of the

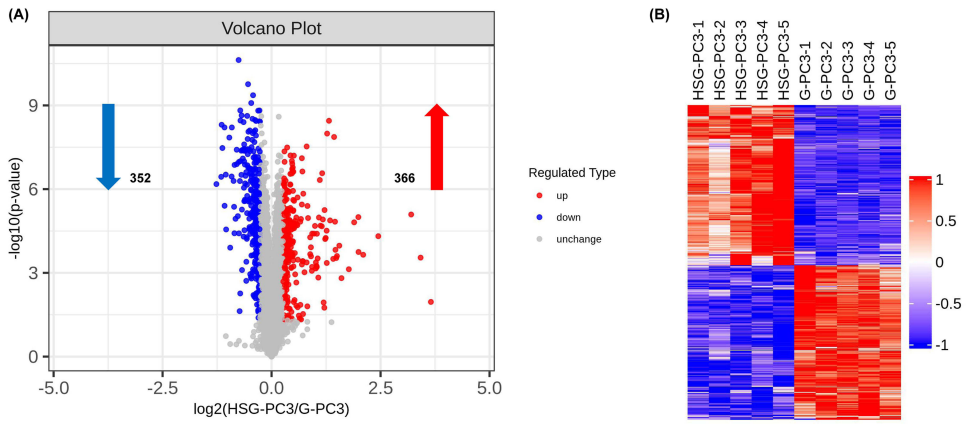

Figure 5 Proteomic response between geraniol and HA-SS-geraniol groups. (**A**) Volcano plot of differentially expressed proteins, with red and blue dots representing up-regulated and down-regulated proteins, respectively. Screening criteria: p value <0.05, Fold change>1.2 or <0.833. (**B**) Hierarchical clustering of differentially expressed proteins. Red represents an up-regulated protein, blue represents a down-regulated protein, and gray represents no protein quantitative information.
Abbreviations: G, Geraniol; HSG, HA-SS-Geraniol.

involvement of these differential proteins in PC-3 cells after geraniol and HA-SS-Geraniol treatments, GO mapping and annotation were performed using Blast2Go. The differential proteins were categorized and annotated into three classifications: biological process (BP), molecular function (MF), and cellular component (CC), as shown in (Figure 6B). The top 5 enriched GO terms were all related to the cellular component category, specifically the mitochondrial part, mitochondrial envelope, mitochondrial membrane, mitochondrial inner membrane, and mitochondrial protein complex (Figure 6C). The KEGG pathways were categorized into seven branches: cellular processes, environmental information processing, genetic information processing, human disease, metabolism, organismal systems, and drug development (source: https://www.genome.jp/kegg/pathway.html). We further analyzed the involvement of differential proteins in the metabolism and cellular processes pathways. Based on the enrichment analysis using Fisher's Exact Test, the bar chart illustrates that the top 5 enriched KEGG pathways in which the differential proteins participated are energy metabolism, cell growth and death, cell motility, transport and catabolism, and amino acid metabolism (Figure 6D). Notably, the oxidative phosphorylation pathway was mapped, revealing the down-regulation of several proteins in the NADH dehydrogenase pathway (indicated by dark green labeling) and up-regulation of proteins in the cytochrome c oxidase, cytochrome c and F-type ATPase pathways (indicated by red labeling) (Figure 7). These findings provide insights into the specific protein alterations and their potential implications in energy production and cellular processes.

PPI Analysis

A protein-protein interaction network was constructed to investigate the relationship between the differential proteins. Among these proteins, 25 with the highest degree of connectivity were selected and described in a network using the STRING database. The network was visualized with the proteins represented by their respective gene names (Figure 8). The colored and filled nodes represent query proteins and the first shell of interactors with a known or predicted 3D structure. Blue edges indicate interactions from curated databases of known interactions, while purple edges denote experimentally determined interactions from known interactions. Green edges signify gene neighborhoods of predicted interactions, and red edges indicate gene fusions of predicted interactions. Additionally, blue edges represent gene co-occurrence of predicted interactions, while other edges in yellow represent text mining, and those in black represent co-expression. According to the network, the top 5 proteins with high connectivity were CYCS, OXA1L (CYCS-OXA1L: same degree), SOD2, HSPD1, and ATP5F1A (HSPD1-ATP5F1A: same degree). Additionally, TOMM40, ALB, MRPL3, MRPL2, and MRPL17 (TOMM40-MRPL17: same degree) had significant connectivity. Other proteins with notable connectivity included ATP5F1B, VDAC1, and MRPS7 (ATP5F1B-MRPS7: same degree). Table 1 provides a ranked list of these 25 proteins based on their degree of involvement.

Anti-Tumor Effects of Geraniol and HA-SS-Geraniol in vivo

The control, geraniol, and HA-SS-Geraniol group tumor volumes were recorded on the first day of drug administration. Mice were dissected, and tumors were collected at the end of the treatment (Figure 9A). The tumor volumes in the

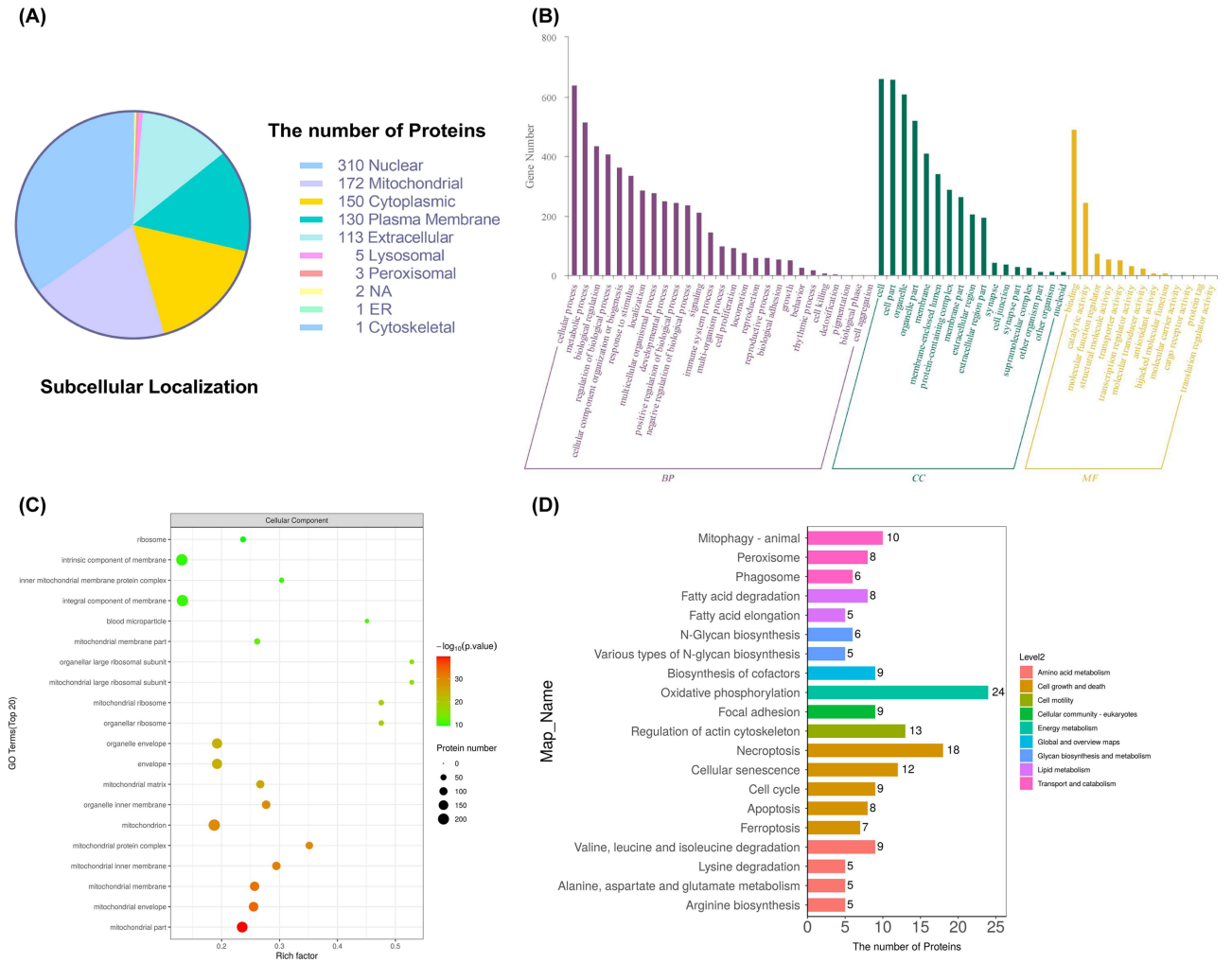

Figure 6 Bioinformatic analysis based on the differentially expressed proteins. (**A**) Subcellular localization of the differentially expressed proteins. (**B**) GO annotations of the differentially expressed proteins in biological processes, molecular function, and cellular components. (**C**) Enrichment analysis of GO terms in the cellular component. (**D**) Top 20 annotations of KEGG pathways related to metabolism and cellular processes.
Abbreviation: ER, endoplasmic reticulum.

geraniol and HA-SS-Geraniol groups were lower than those in the control group. Specifically, the HA-SS-Geraniol group had an average volume of half as low as the control group. Although the solid tumors did not completely disappear, the growth rate of the HA-SS-Geraniol group was significantly slowed down, with a tumor growth inhibitory ratio of 54.0% compared to 9.2% in the geraniol group (Figure 9B).

Discussion

Developing targeted delivery systems has revolutionized cancer treatment by allowing more precise and effective treatment strategies. These delivery systems can be engineered to recognize and bind to specific cell surface receptors or antigens overexpressed on cancer cells, such as the interaction between HA and CD44.[31,32] Additionally, using disulfide bonds in targeted delivery system design has improved target specificity and bioavailability and potentially enhanced therapeutic efficacy.[33] The high expression of CD44 on PC-3 prostate cancer cells allows for targeted delivery of the HA-SS-geraniol conjugate, exploiting the overexpression of CD44 receptors in cancer cells. This targeted delivery is further enhanced by the selective disruption of disulfide bonds within the HA-SS-geraniol conjugate, promoting the release of geraniol in response to the differential glutathione (GSH) contents between normal and cancer cells.[34–36] The stable conjugate, formed by linking hyaluronic acid (HA) and geraniol via disulfide bonds, self-assembles into

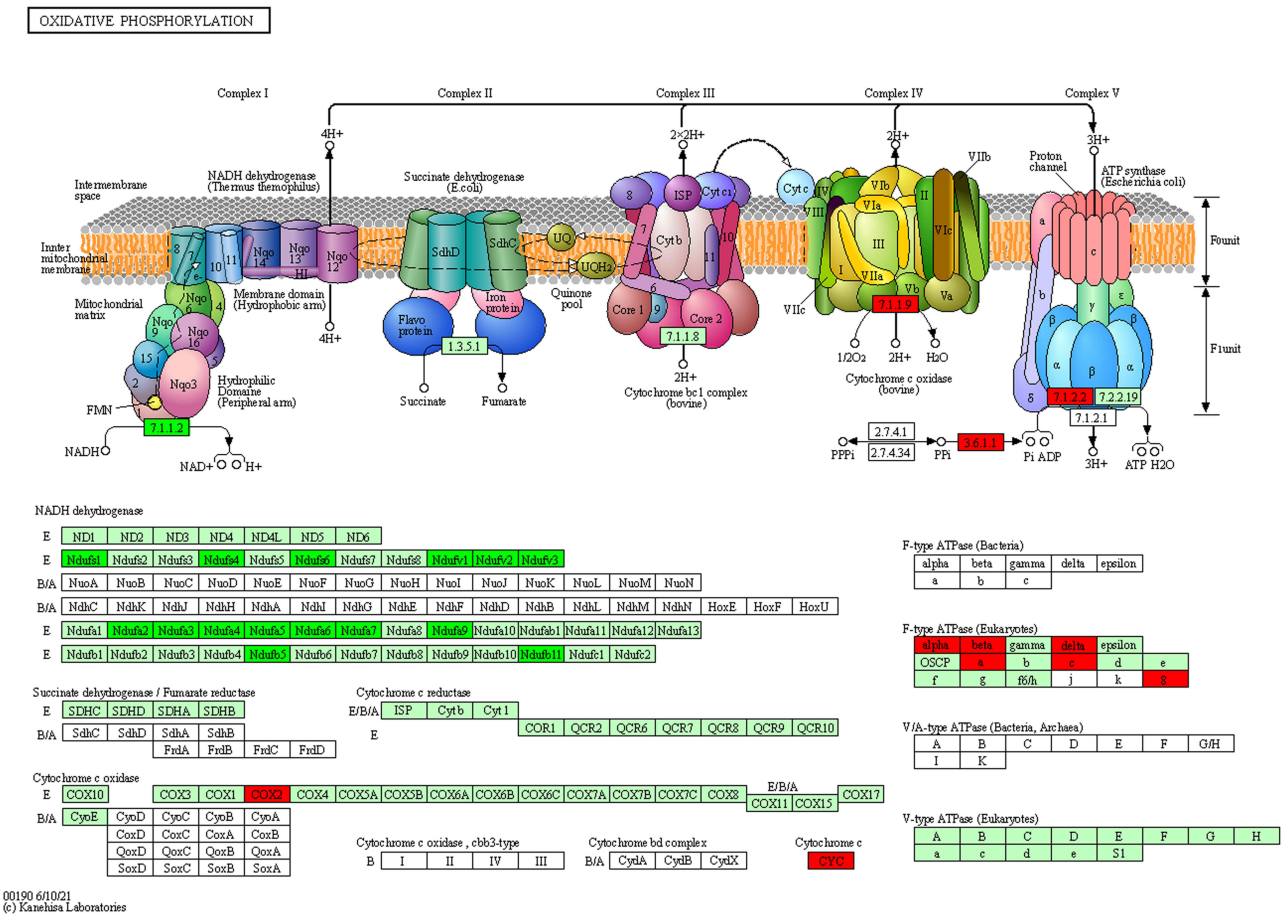

Figure 7 Differentially expressed proteins elucidated in the KEGG mapping of the oxidative phosphorylation pathway.

nanoparticles in aqueous solution, enabling targeted delivery and controlled release of geraniol specifically in the tumor microenvironment. Previous studies have demonstrated the efficacy of HA-SS-geraniol conjugate in liver cancer and their potential for selective targeting and stimuli-responsive release of geraniol.[29] These properties make HA-SS-geraniol an attractive candidate for targeted anti-cancer therapy. Our in vitro cytotoxicity assay confirmed the significant anti-cancer effect of HA-SS-geraniol on human PC-3 prostate cancer cells, highlighting its potential for enhanced therapeutic outcomes in cancer treatment.

The loss of mitochondrial membrane potential can trigger various cellular stress responses, including the release of cytochrome c, which eliminates damaged mitochondria.[37,38] However, this process may ultimately lead to apoptosis, a programmed cell death.[39,40] In our study, we evaluated the efficacy of the HA-SS-Geraniol conjugate in an in vitro model of prostate cancer. We observed a significant loss of mitochondrial membrane potential and an apoptotic effect, as determined by flow cytometry. Our data support the potential of mitochondria-mediated apoptosis as a mechanism of cell death induced by the HA-SS-Geraniol conjugate. Previous studies have shown that geraniol can arrest PC-3 prostate cancer cells in the G_2 phase and down-regulate E2F8 as a potential mechanism.[41] Our data showed a consistent result and suggested a potential role for similar transcription regulation in the anti-cancer effect of the HA-SS-Geraniol conjugate.

Our study aimed to investigate the mechanisms underlying the anti-cancer efficacy of HA-SS-Geraniol on prostate cancer cells. Proteomic analysis was conducted to identify differential proteins following treatment with geraniol and HA-SS-Geraniol. A total of 718 differential proteins were identified in our study. Among these proteins, we observed up-regulation of specific proteins in the peroxisome, such as PEX14, a peroxisome membrane protein. This up-regulation may affect the peroxisomal

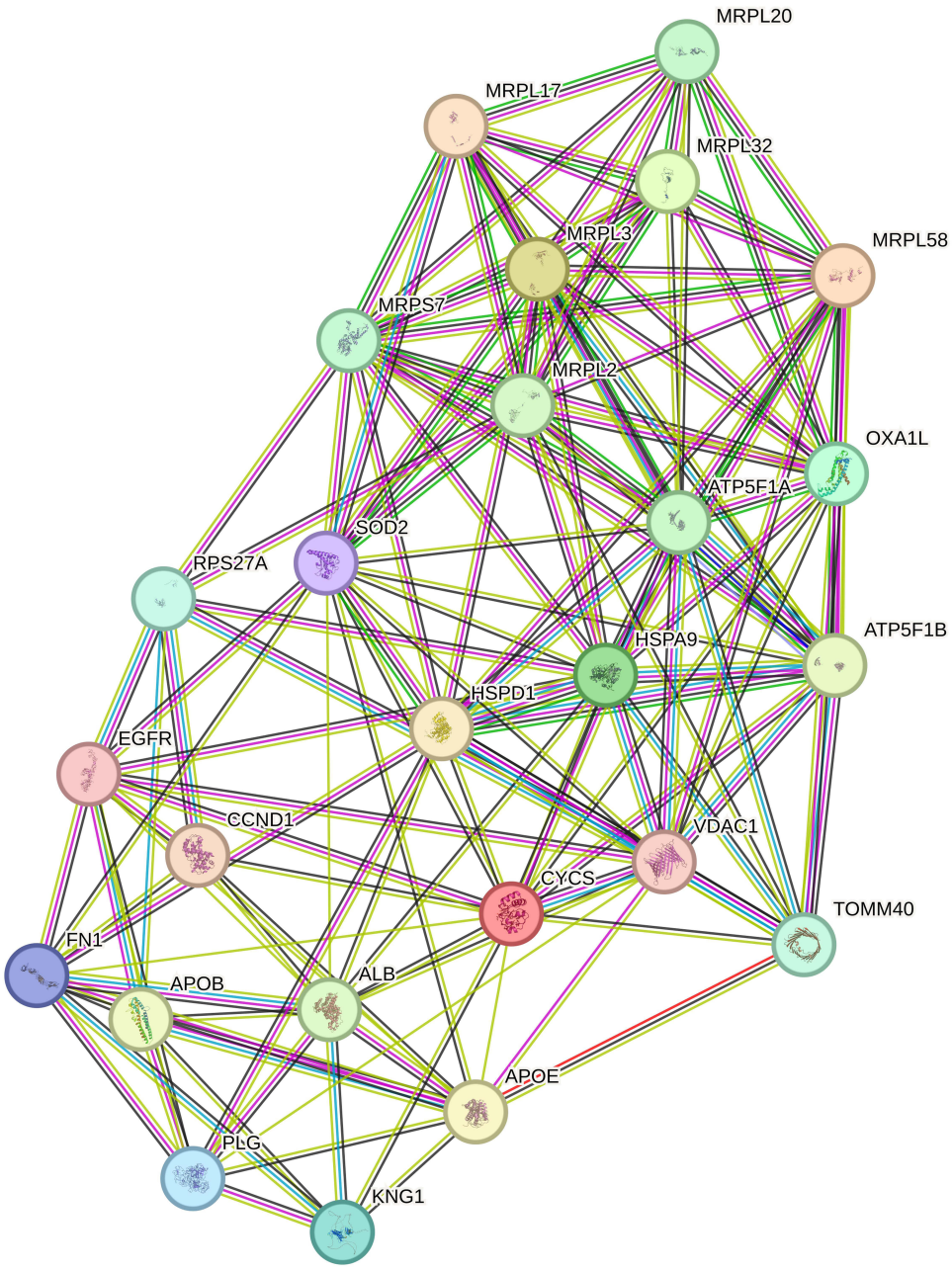

Figure 8 Protein-protein interaction network of the top 25 differentially expressed proteins with the highest connectivity degree.

import of catalase and contribute to oxidative stress.[42] Disruption of peroxisomal function can lead to an imbalance in reactive oxygen species (ROS) and mitochondrial dysfunction.[43] Furthermore, we observed the down-regulation of specific proteins involved in the mitochondrial electron transport chain. For instance, NDUFA5 and NDUFA11, subunits of the NADH dehydrogenase (ubiquinone) complex, play a crucial role in the assembly and activity of the mitochondrial electron transport chain. The down-regulation of these complex subunits may disrupt the normal functioning of the electron transport chain, potentially impacting cellular energy production and metabolism.[44–46] Subcellular localization prediction of the differential proteins revealed that the most significant organelles affected were the nucleus and mitochondria, where crucial cellular processes occur. Previous studies have demonstrated that nuclear-mitochondrial interactions can influence energy production, metabolism, cell growth, and death.[47] Based on these findings, we further investigated whether the mitochondria function was affected by HA-SS-Geraniol treatment.

Table 1 Topological Information of the 25 Differentially Expressed Proteins with the Highest Connectivity Degree

Accession	Protein Name	Gene Name	Degree
P99999	Cytochrome c	CYCS	15
Q15070	Mitochondrial inner membrane protein OXA1L	OXA1L	15
P04179	Superoxide dismutase [Mn], mitochondrial	SOD2	14
P10809	60 kDa heat shock protein, mitochondrial	HSPD1	13
P25705	ATP synthase subunit alpha, mitochondrial	ATP5F1A	13
O96008	Mitochondrial import receptor subunit TOM40 homolog	TOMM40	12
P02768	Albumin	ALB	12
P09001	39S ribosomal protein L3, mitochondrial	MRPL3	12
Q5T653	39S ribosomal protein L2, mitochondrial	MRPL2	12
Q9NRX2	39S ribosomal protein L17, mitochondrial	MRPL17	12
P06576	ATP synthase subunit beta, mitochondrial	ATP5F1B	11
P21796	Voltage-dependent anion-selective channel protein 1	VDAC1	11
Q9Y2R9	28S ribosomal protein S7, mitochondrial	MRPS7	11
P02649	Apolipoprotein E	APOE	10
P38646	Stress-70 protein, mitochondrial	HSPA9	10
P02751	Fibronectin	FN1	9
Q9BYC9	39S ribosomal protein L20, mitochondrial	MRPL20	9
P00533	Epidermal growth factor receptor	EGFR	8
P00747	Plasminogen	PLG	8
P62979	Ubiquitin-40S ribosomal protein S27a	RPS27A	8
Q9BYC8	39S ribosomal protein L32, mitochondrial	MRPL32	8
P04114	Apolipoprotein B-100	APOB	7
Q14197	Peptidyl-tRNA hydrolase ICT1, mitochondrial	MRPL58	7
P01042	Kininogen-1	KNG1	6
P24385	G1/S-specific cyclin-D1	CCND1	5

The results of the GO and KEGG enrichment analyses indicated that the function of mitochondria appeared to be the primary change affected by HA-SS-Geraniol treatment. Previous studies have suggested that the mitochondria-mediated apoptosis pathway may be closely related to and affected by various factors, including insufficient energy supply resulting from impaired ATP synthesis, overexpression of reactive oxygen species due to oxidative stress, and abnormal structure and function of the cell membrane caused by lipid metabolism disorders.[48–50] Our findings demonstrated a significant association between the differential proteins identified in the mitochondria and key pathways involved in energy metabolism, cell growth and death, amino acid metabolism, and lipid metabolism. Based on these observations, we speculate that the anti-cancer mechanism of HA-SS-Geraniol may involve the induction of mitochondrial dysfunction through the apoptosis pathway,

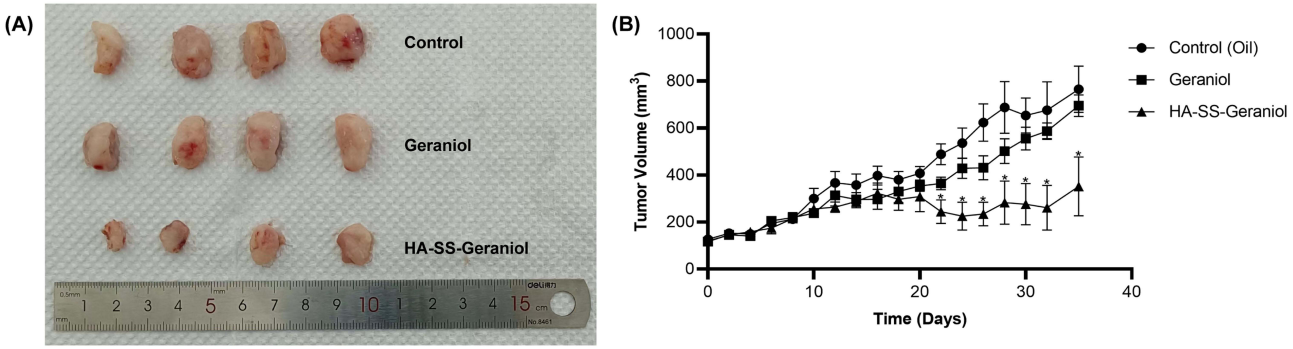

Figure 9 HA-SS-geraniol significantly suppressed tumor progression. (**A**) The representative images of isolated tumors at the end of treatments. (**B**) Average growth curve of xenograft tumor volume. (Mean ± SEM; n = 4; * p < 0.05).

disruptions in ATP synthesis, oxidative stress, and alterations in lipid metabolism, all of which are influenced by the actions of the identified differential proteins. Furthermore, oxidative phosphorylation mapping data analysis reveals substantial changes in cellular energy metabolism and mitochondrial function. The down-regulation of the NADH dehydrogenase pathway suggests a potential disruption in the electron transport chain and oxidative phosphorylation, indispensable for normal energy production.[51] Conversely, the up-regulation of cytochrome c oxidase, cytochrome c, and F-type ATPase indicates compensatory mechanisms to enhance energy production and support cell survival.[52–54] This up-regulation likely reflects an increased demand for energy and ATP synthesis in response to the drug treatment. Nevertheless, it is important to note that the up-regulation of cytochrome c oxidase and cytochrome c can affect reactive oxygen species (ROS) levels and mitochondrial function.[55,56] Treatment with HA-SS-Geraniol may result in elevated ROS levels as cancer cells attempt to restore cellular homeostasis. These increased ROS levels have the potential to induce apoptosis and disrupt mitochondrial function.[57] Our in vitro study's findings support the induction of mitochondria-mediated apoptosis following HA-SS-Geraniol treatment. However, further investigation is necessary to fully comprehend the intricate interplay between ROS, apoptosis, and mitochondrial function in response to HA-SS-Geraniol treatment and explore potential therapeutic implications.

The PPI network analysis further emphasized the impact of HA-SS-Geraniol on mitochondrial dysfunction. Our results revealed several core differential proteins that provided evidence for the disruption of mitochondria-related functions. For instance, CYCS, also known as cytochrome c, is an electron carrier protein in the space between the inner and outer mitochondrial membranes. It is crucial for stimulating caspase activation and triggering cell death.[58] Mitochondrial superoxide dismutase (SOD2) is an essential enzyme that handles reactive oxygen species (ROS) and regulates cell signaling within the mitochondrial matrix.[59] OXA1 is a mitochondrial inner membrane protein vital for the activity and assembly of cytochrome oxidase, which may affect respiration.[60] These proteins exhibited significant connectivity in our study, proving their involvement in modulating mitochondrial function.

The in vivo study of HA-SS-Geraniol demonstrated its ability to inhibit tumor proliferation and induce apoptosis. These findings were consistent with our in vitro apoptosis study, further confirming the anti-cancer effectiveness of HA-SS-Geraniol. Additionally, the in vivo toxicity study confirmed the significant safety profile of geraniol and provided valuable information regarding appropriate dosage administration and treatment cycles. The HE data also contributed to optimizing HA-SS-Geraniol preparation for future studies.

Conclusion

In conclusion, our study provides evidence supporting the potential therapeutic use of HA-conjugated geraniol, specifically HA-SS-Geraniol, for cancer treatment. Our findings demonstrate that HA-SS-Geraniol significantly enhances cytotoxicity in prostate PC-3 cells, leading to the loss of mitochondrial membrane potential and cell cycle arrest in the G_2 phase. Additionally, our proteomic study supports the hypothesis that mitochondria-mediated apoptosis is a key pathway through which HA-SS-Geraniol induces cell death. Furthermore, the in vivo study confirms the effectiveness of HA-SS-Geraniol in inhibiting tumor growth.

Acknowledgments

This work was supported by the Wenzhou-Kean University Internal Faculty Research Support Program (IRSPG202102), International Collaborative Research Program (ICRP202201), Wenzhou-Kean University Student Partnering with Faculty Research Program, WKUSPF2023023.

Disclosure

The authors report no conflicts of interest in this work.

References

1. Chhikara BS, Parang K. Global Cancer Statistics 2022: the trends projection analysis. *Chem Biol Lett*. 2023;10(1):451.
2. Xia C, Dong X, Li H, et al. Cancer statistics in China and United States, 2022: profiles, trends, and determinants. *Chin Med J (Engl)*. 2022;135(5):584–590. doi:10.1097/CM9.0000000000002108
3. Muhamad N, Plengsuriyakarn T, Na-Bangchang K. Application of active targeting nanoparticle delivery system for chemotherapeutic drugs and traditional/herbal medicines in cancer therapy: a systematic review. *Int J Nanomed*. 2018;13:3921–3935. doi:10.2147/IJN.S165210

4. Danhier F, Feron O, Preat V. To exploit the tumor microenvironment: passive and active tumor targeting of nanocarriers for anti-cancer drug delivery. *J Control Release*. 2010;148(2):135–146. doi:10.1016/j.jconrel.2010.08.027
5. Wang CY, Yamada H, Morton KC, Zukowski K, Lee MS, King CM. Induction of repair synthesis of DNA in mammary and urinary bladder epithelial cells by N-hydroxy derivatives of carcinogenic arylamines. *Cancer Res*. 1988;48(15):4227–4232.
6. Niu B, Liao K, Zhou Y, et al. Application of glutathione depletion in cancer therapy: enhanced ROS-based therapy, ferroptosis, and chemotherapy. *Biomaterials*. 2021;277:121110. doi:10.1016/j.biomaterials.2021.121110
7. Zou L, Liu X, Li J, et al. Redox-sensitive carrier-free nanoparticles self-assembled by disulfide-linked paclitaxel-tetramethylpyrazine conjugate for combination cancer chemotherapy. *Theranostics*. 2021;11(9):4171–4186. doi:10.7150/thno.42260
8. Li J, Burgess DJ. Nanomedicine-based drug delivery towards tumor biological and immunological microenvironment. *Acta Pharm Sin B*. 2020;10 (11):2110–2124. doi:10.1016/j.apsb.2020.05.008
9. Yang S, Gao H. Nanoparticles for modulating tumor microenvironment to improve drug delivery and tumor therapy. *Pharmacol Res*. 2017;126:97–108. doi:10.1016/j.phrs.2017.05.004
10. Zhao Y, Zhang T, Duan S, Davies NM, Forrest ML. CD44-tropic polymeric nanocarrier for breast cancer targeted rapamycin chemotherapy. *Nanomedicine*. 2014;10(6):1221–1230. doi:10.1016/j.nano.2014.02.015
11. Mohammed M, Devnarain N, Elhassan E, Govender T. Exploring the applications of hyaluronic acid-based nanoparticles for diagnosis and treatment of bacterial infections. *Wiley Interdiscip Rev Nanomed Nanobiotechnol*. 2022;14(4):e1799. doi:10.1002/wnan.1799
12. Hassn Mesrati M, Syafruddin SE, Mohtar MA, Syahir A. CD44: a Multifunctional Mediator of Cancer Progression. *Biomolecules*. 2021;11 (12):1850. doi:10.3390/biom11121850
13. Morath I, Hartmann TN, Orian-Rousseau V. CD44: more than a mere stem cell marker. *Int J Biochem Cell Biol*. 2016;81(Pt A):166–173. doi:10.1016/j.biocel.2016.09.009
14. Li W, Qian L, Lin J, et al. CD44 regulates prostate cancer proliferation, invasion and migration via PDK1 and PFKFB4. *Oncotarget*. 2017;8 (39):65143–65151. doi:10.18632/oncotarget.17821
15. Korski K, Malicka-Durczak A, Breborowicz J. Expression of stem cell marker CD44 in prostate cancer biopsies predicts cancer grade in radical prostatectomy specimens. *Pol J Pathol*. 2014;65(4):291–295. doi:10.5114/pjp.2014.48190
16. Ali Abdalla YO, Subramaniam B, Nyamathulla S, et al. Natural Products for Cancer Therapy: a Review of Their Mechanism of Actions and Toxicity in the Past Decade. *J Trop Med*. 2022;2022:5794350. doi:10.1155/2022/5794350
17. Fatima K, Wani ZA, Meena A, Luqman S. Geraniol exerts its antiproliferative action by modulating molecular targets in lung and skin carcinoma cells. *Phytother Res*. 2021;35(7):3861–3874. doi:10.1002/ptr.7094
18. Maczka W, Winska K, Grabarczyk M. One Hundred Faces of Geraniol. *Molecules*. 2020;25(14):3303. doi:10.3390/molecules25143303
19. Choi HS, Song HS, Ukeda H, Sawamura M. Radical-scavenging activities of citrus essential oils and their components: detection using 1,1-diphenyl-2-picrylhydrazyl. *J Agric Food Chem*. 2000;48(9):4156–4161. doi:10.1021/jf000227d
20. El-Ganainy SO, Shehata AM, El-Mallah A, Abdallah D, Mohy El-Din MM. Geraniol suppresses tumour growth and enhances chemosensitivity of 5-fluorouracil on breast carcinoma in mice: involvement of miR-21/PTEN signalling. *J Pharm Pharmacol*. 2023;75(8):1130–1139. doi:10.1093/jpp/rgad060
21. Galle M, Crespo R, Kladniew BR, Villegas SM, Polo M, de Bravo MG. Suppression by geraniol of the growth of A549 human lung adenocarcinoma cells and inhibition of the mevalonate pathway in culture and in vivo: potential use in cancer chemotherapy. *Nutr Cancer*. 2014;66(5):888–895. doi:10.1080/01635581.2014.916320
22. Carnesecchi S, Bras-Goncalves R, Bradaia A, et al. Geraniol, a component of plant essential oils, modulates DNA synthesis and potentiates 5-fluorouracil efficacy on human colon tumor xenografts. *Cancer Lett*. 2004;215(1):53–59. doi:10.1016/j.canlet.2004.06.019
23. Jin X, Sun J, Miao X, Liu G, Zhong D. Inhibitory effect of geraniol in combination with gemcitabine on proliferation of BXPC-3 human pancreatic cancer cells. *J Int Med Res*. 2013;41(4):993–1001. doi:10.1177/0300060513480919
24. Chaudhary SC, Siddiqui MS, Athar M, Alam MS. Geraniol inhibits murine skin tumorigenesis by modulating COX-2 expression, Ras-ERK1/2 signaling pathway and apoptosis. *J Appl Toxicol*. 2013;33(8):828–837. doi:10.1002/jat.2739
25. Crespo R, Montero Villegas S, Abba MC, de Bravo MG, Polo MP. Transcriptional and posttranscriptional inhibition of HMGCR and PC biosynthesis by geraniol in 2 Hep-G2 cell proliferation linked pathways. *Biochem Cell Biol*. 2013;91(3):131–139. doi:10.1139/bcb-2012-0076
26. Ahmad ST, Arjumand W, Seth A, et al. Preclinical renal cancer chemopreventive efficacy of geraniol by modulation of multiple molecular pathways. *Toxicology*. 2011;290(1):69–81. doi:10.1016/j.tox.2011.08.020
27. Kim SH, Park EJ, Lee CR, et al. Geraniol induces cooperative interaction of apoptosis and autophagy to elicit cell death in PC-3 prostate cancer cells. *Int J Oncol*. 2012;40(5):1683–1690. doi:10.3892/ijo.2011.1318
28. Kim SH, Bae HC, Park EJ, et al. Geraniol inhibits prostate cancer growth by targeting cell cycle and apoptosis pathways. *Biochem Biophys Res Commun*. 2011;407(1):129–134. doi:10.1016/j.bbrc.2011.02.124
29. Duan S, Xia Y, Tian X, et al. A multi-bioresponsive self-assembled nano drug delivery system based on hyaluronic acid and geraniol against liver cancer. *Carbohydr Polym*. 2023;310:120695. doi:10.1016/j.carbpol.2023.120695
30. Wisniewski JR, Zougman A, Nagaraj N, Mann M. Universal sample preparation method for proteome analysis. *Nat Methods*. 2009;6(5):359–362. doi:10.1038/nmeth.1322
31. Mitra AK, Agrahari V, Mandal A, et al. Novel delivery approaches for cancer therapeutics. *J Control Release*. 2015;219:248–268. doi:10.1016/j.jconrel.2015.09.067
32. Kesharwani P, Chadar R, Sheikh A, Rizg WY, Safhi AY. CD44-Targeted Nanocarrier for Cancer Therapy. *Front Pharmacol*. 2021;12:800481. doi:10.3389/fphar.2021.800481
33. Shende P, Deshpande G. Disulfide Bond-Responsive Nanotherapeutic Systems for the Effective Payload in Cancer Therapy. *Curr Pharm Des*. 2020;26(41):5353–5361. doi:10.2174/1381612826666200707131006
34. Senbanjo LT, AlJohani H, Majumdar S, Chellaiah MA. Characterization of CD44 intracellular domain interaction with RUNX2 in PC3 human prostate cancer cells. *Cell Commun Signal*. 2019;17(1):80. doi:10.1186/s12964-019-0395-6
35. Feng J, Xu Z, Liu F, et al. Versatile Catalytic Deoxyribozyme Vehicles for Multimodal Imaging-Guided Efficient Gene Regulation and Photothermal Therapy. *ACS Nano*. 2018;12(12):12888–12901. doi:10.1021/acsnano.8b08101
36. Ganesh S, Iyer AK, Morrissey DV, Amiji MM. Hyaluronic acid based self-assembling nanosystems for CD44 target mediated siRNA delivery to solid tumors. *Biomaterials*. 2013;34(13):3489–3502. doi:10.1016/j.biomaterials.2013.01.077

37. Lockshin RA, Zakeri Z. Apoptosis, autophagy, and more. *Int J Biochem Cell Biol*. 2004;36(12):2405–2419. doi:10.1016/j.biocel.2004.04.011
38. Eisenberg-Lerner A, Bialik S, Simon HU, Kimchi A. Life and death partners: apoptosis, autophagy and the cross-talk between them. *Cell Death Differ*. 2009;16(7):966–975. doi:10.1038/cdd.2009.33
39. Gottlieb E, Armour SM, Harris MH, Thompson CB. Mitochondrial membrane potential regulates matrix configuration and cytochrome c release during apoptosis. *Cell Death Differ*. 2003;10(6):709–717. doi:10.1038/sj.cdd.4401231
40. Vasan K, Clutter M, Fernandez Dunne S, et al. Genes Involved in Maintaining Mitochondrial Membrane Potential Upon Electron Transport Chain Disruption. *Front Cell Dev Biol*. 2022;10:781558. doi:10.3389/fcell.2022.781558
41. Lee S, Park YR, Kim SH, et al. Geraniol suppresses prostate cancer growth through down-regulation of E2F8. *Cancer Med*. 2016;5(10):2899–2908. doi:10.1002/cam4.864
42. Okumoto K, El Shermely M, Natsui M, et al. The peroxisome counteracts oxidative stresses by suppressing catalase import via Pex14 phosphorylation. *Elife*. 2020;9:e55896. doi:10.7554/eLife.55896
43. Cipolla CM, Lodhi IJ. Peroxisomal Dysfunction in Age-Related Diseases. *Trends Endocrinol Metab*. 2017;28(4):297–308. doi:10.1016/j.tem.2016.12.003
44. Stroud DA, Surgenor EE, Formosa LE, et al. Accessory subunits are integral for assembly and function of human mitochondrial complex I. *Nature*. 2016;538(7623):123–126. doi:10.1038/nature19754
45. Emelyanova L, Preston C, Gupta A, et al. Effect of Aging on Mitochondrial Energetics in the Human Atria. *J Gerontol a Biol Sci Med Sci*. 2018;73(5):608–616. doi:10.1093/gerona/glx160
46. Reinson K, Kovacs-Nagy R, Oiglane-Shlik E, et al. Diverse phenotype in patients with complex I deficiency due to mutations in NDUFB11. *Eur J Med Genet*. 2019;62(11):103572. doi:10.1016/j.ejmg.2018.11.006
47. Walker BR, Moraes CT. Nuclear-Mitochondrial Interactions. *Biomolecules*. 2022;12(3):427. doi:10.3390/biom12030427
48. Srivastava A, Srivastava P, Mathur S, et al. Lipid Metabolism and Mitochondria: cross Talk in Cancer. *Curr Drug Targets*. 2022;23(6):606–627. doi:10.2174/1389450122666210824144907
49. Guo C, Sun L, Chen X, Zhang D. Oxidative stress, mitochondrial damage and neurodegenerative diseases. *Neural Regen Res*. 2013;8(21):2003–2014. doi:10.3969/j.issn.1673-5374.2013.21.009
50. Wang C, Youle RJ. The role of mitochondria in apoptosis*. *Annu Rev Genet*. 2009;43:95–118. doi:10.1146/annurev-genet-102108-134850
51. Walker MA, Tian R. NAD(H) in mitochondrial energy transduction: implications for health and disease. *Curr Opin Physiol*. 2018;3:101–109. doi:10.1016/j.cophys.2018.03.011
52. Fontanesi F, Soto IC, Barrientos A. Cytochrome c oxidase biogenesis: new levels of regulation. *IUBMB Life*. 2008;60(9):557–568. doi:10.1002/iub.86
53. Welchen E, Gonzalez DH. Cytochrome c, a hub linking energy, redox, stress and signaling pathways in mitochondria and other cell compartments. *Physiol Plant*. 2016;157(3):310–321. doi:10.1111/ppl.12449
54. Kuhlbrandt W. Structure and Mechanisms of F-Type ATP Synthases. *Annu Rev Biochem*. 2019;88(1):515–549. doi:10.1146/annurev-biochem-013118-110903
55. Atlante A, Calissano P, Bobba A, Azzariti A, Marra E, Passarella S. Cytochrome c is released from mitochondria in a reactive oxygen species (ROS)-dependent fashion and can operate as a ROS scavenger and as a respiratory substrate in cerebellar neurons undergoing excitotoxic death. *J Biol Chem*. 2000;275(47):37159–37166. doi:10.1074/jbc.M002361200
56. Vempati UD, Diaz F, Barrientos A, et al. Role of cytochrome C in apoptosis: increased sensitivity to tumor necrosis factor alpha is associated with respiratory defects but not with lack of cytochrome C release. *Mol Cell Biol*. 2007;27(5):1771–1783. doi:10.1128/MCB.00287-06
57. Redza-Dutordoir M, Averill-Bates DA. Activation of apoptosis signalling pathways by reactive oxygen species. *Biochim Biophys Acta*. 2016;1863(12):2977–2992. doi:10.1016/j.bbamcr.2016.09.012
58. Jiang X, Wang X. Cytochrome C-mediated apoptosis. *Annu Rev Biochem*. 2004;73:87–106. doi:10.1146/annurev.biochem.73.011303.073706
59. Palma FR, He C, Danes JM, et al. Mitochondrial Superoxide Dismutase: what the Established, the Intriguing, and the Novel Reveal About a Key Cellular Redox Switch. *Antioxid Redox Signal*. 2020;32(10):701–714. doi:10.1089/ars.2019.7962
60. Bonnefoy N, Kermorgant M, Groudinsky O, Minet M, Slonimski PP, Dujardin G. Cloning of a human gene involved in cytochrome oxidase assembly by functional complementation of an oxa1- mutation in Saccharomyces cerevisiae. *Proc Natl Acad Sci U S A*. 1994;91(25):11978–11982. doi:10.1073/pnas.91.25.11978